Transmembrane Peptide-Induced Lipid Sorting and Mechanism of L_α-to-Inverted Phase Transition Using Coarse-Grain Molecular Dynamics

Steve O. Nielsen,* Carlos F. Lopez,* Ivaylo Ivanov,* Preston B. Moore,[†] John C. Shelley,[‡] and Michael L. Klein*

*Center for Molecular Modeling and Department of Chemistry, University of Pennsylvania, Philadelphia, Pennsylvania; [†]Department of Chemistry and Biochemistry, University of the Sciences in Philadelphia, Philadelphia, Pennsylvania; and [‡]Schrödinger Inc., Portland, Oregon

ABSTRACT   Molecular dynamics results are presented for a coarse-grain model of 1,2-di-n-alkanoyl-sn-glycero-3-phosphocholine, water, and a capped cylindrical model of a transmembrane peptide. We first demonstrate that different alkanoyl-length lipids are miscible in the liquid-disordered lamellar (L_α) phase. The transmembrane peptide is constructed of hydrophobic sites with hydrophilic caps. The hydrophobic length of the peptide is smaller than the hydrophobic thickness of a bilayer consisting of an equal mixture of long and short alkanoyl tail lipids. When incorporated into the membrane, a meniscus forms in the vicinity of the peptide and the surrounding area is enriched in the short lipid. The meniscus region draws water into it. In the regions that are depleted of water, the bilayers can fuse. The lipid headgroups then rearrange to solvate the newly formed water pores, resulting in an inverted phase. This mechanism appears to be a viable pathway for the experimentally observed L_α-to-inverse hexagonal (H_{II}) peptide-induced phase transition.

INTRODUCTION

Biological membranes display a daunting compositional diversity that includes zwitterionic and anionic phospholipids, galactolipids, cholesterol, and transmembrane ion channels. Membrane models serve as a simplified framework in which to explore individual structural and dynamical aspects of membranes. Experimentally, such model systems consist of different lipid species and may contain cholesterol or a transmembrane peptide (Finegold, 1993). Theoretically, the main approaches to study membranes are through statistical thermodynamics as exemplified by Safran (1994), wherein Ginzburg-Landau expansions of the free energy are considered, or through classical all-atom molecular dynamics (MD) simulations (Scott, 2002). Due to the traditionally fast timescales accessible to MD simulations, the study of lipid miscibility has been largely ignored. Through the use of new methodologies we present a study of a model miscible lipid system.

It has been shown that various lipid molecule types present on a membrane can result in subdomain formation within the lipid membrane. Bilayer microdomains have been observed under different conditions such as in cholesterol mixtures (in which case they are called rafts) or a transmembrane peptide. Subdomains may also form under surface-pressure modifications in a Langmuir monolayer (LM) (Gopal and Lee, 2001). Incidentally, domain formation between different phases of the same lipid species can be observed in LMs (Schief et al., 2000). Most of these systems are too complicated and cannot be studied using current computational techniques with atomistic detail.

To gain some insights about the interactions between different lipids in a bilayer and their interactions with constructs that perturb the bilayer environment, we explore two different, yet complementary, effects that a short cylindrical peptide can induce in a mixed-lipid system. We limit our study to effects arising solely from hydrophobic mismatch. The first process we study is domain formation in an otherwise mixed-lipid bilayer. The second is the transition from the lamellar L_α phase to an inverted phase. In both cases the driving force for the reorganization of the system is the extent of hydrophobic mismatch between the lipid bilayer and the peptide.

It has been proposed that lipid domains of different hydrophobic thickness are used to sort membrane proteins based on the length of their transmembrane domains (Sprong et al., 2001), but this picture is misleading because it is known that proteins themselves passively induce lipid domain formation (Dumas et al., 1999). The hydrophobic matching principle states that in the immediate vicinity of the peptide there is an accumulation of the lipid that is hydrophobically best matched (Dumas et al., 1997). Typically one pictures the bilayer-spanning part of a transmembrane peptide as a hydrophobic alpha-helix with caps that preferentially associate with the interfacial lipid headgroup-water region. Lipid bilayers are more easily deformed than transmembrane proteins (de Planque et al, 2001), and the assumption is made that the bilayer deforms to match the hydrophobic length of the protein (Harroun et al., 1999a), leaving the protein virtually unchanged. Theoretical considerations point to a range of effects that contribute to the free

energy in the presence of such a peptide inclusion. These consist of elastic acyl chain stretching/compression, surface tension terms accounting for the average interfacial area per molecule, curvature contributions from the formation of a meniscus around the inclusion, and tilt modulus of the acyl chains (Fattal and Ben-Shaul, 1993; Sens and Safran, 2000; May and Ben-Shaul, 1999; Gil et al., 1998; Wahab et al., 2001; Nielsen et al., 1998; Duque et al., 2002).

At high concentration, transmembrane peptides can have more dramatic effects on the membrane structure. Short peptides, namely peptides whose hydrophobic length is shorter than the bilayer thickness, have been shown to induce phase transitions from the lamellar to an inverted phase (Killian et al., 1996). Long peptides do not have this effect—they tilt instead, and the lipid remains in the lamellar phase (Li, 2000; Killian et al., 1996). If the peptide hydrophobic length is grossly mismatched from the membrane thickness, the peptide may fail to insert (de Planque et al, 2001; van der Wel et al., 2000). More generally, inverted phases can be induced in phospholipid membranes by dehydration (Yang and Huang, 2002), heating (Rappolt et al., 2003), the addition of divalent cations (Ortiz et al., 1999), the addition of lipids of negative intrinsic curvature (Zimmerberg and Chernomordik, 1999; Li and Schick, 2000; Marrink and Mark, 2003), or the addition of synthetic peptide (Killian et al., 1996).

For the tryptophan-capped synthetic peptides used experimentally (Killian et al., 1996), the two dominant effects of the peptide are thought to come from its hydrophobic length and from the tryptophan anchoring residues (Petrache et al., 2002). The bulky multiple tryptophan groups at each end of the peptide are thought to play a dual role in anchoring the peptide ends in the headgroup region of the bilayer, and in preventing peptide aggregation. Since there should be a lipid-mediated peptide-peptide attractive force present in the system, aggregation is otherwise a strong possibility (Harroun et al., 1999a,b; Gil et al., 1998; Kralchevsky and Nagayama, 2000; Sharpe et al., 2002; Weikl, 2001; Lagüe et al., 1998, 2001; Dan et al., 1993). We avoid the possibility of aggregation in this work by considering only a single peptide assembly per unit cell. This, together with the orthorhombic cell geometry, does not permit the experimentally observed inverse hexagonal (H_{II}) phase (Killian et al., 1996) to form; rather we observe the formation of an inverted phase with a different symmetry.

Neither the existing experimental nor theoretical studies shed light on the mechanism that could drive such a phase transition (Killian et al., 1996; May and Ben-Shaul, 1999). Rather, the stability of the resulting H_{II} phase is justified a posteriori. In this study, which uses coarse-grain MD, we propose a mechanism wherein the transbilayer peptide induces the formation of a meniscus, causing the accretion of interbilayer water into the meniscus region. This movement depletes the water layer far from the peptide, allowing the bilayers in these regions to fuse. This fusion

event pinches off the water sheets, trapping the water in cylindrical pores, which are the hallmark of inverted phases. The headgroups then rearrange to solvate these water pores.

METHODS

Domain formation cannot currently be studied using fully atomistic MD. The use of a coarse grain method is necessary to access the timescale needed for lateral diffusion of membrane species in the bilayer plane. An efficient coarse-grain model has been developed for phospholipids and water which offers a speedup of roughly five orders of magnitude over all-atom MD (Nielsen et al., 2004; Shelley et al., 2001a,b; Shelley, 2003).

A series of 1,2-di-n-alkanoyl-sn-glycero-3-phosphocholine lipids (DC_nPC) are used; namely $DC_{11}PC$ (referred to as the short lipid), $DC_{14}PC$ (commonly known as DMPC), $DC_{17}PC$, and $DC_{29}PC$ (referred to as the long lipid). Coarse-grain $DC_{14}PC$ and water parameters have been developed and characterized (Shelley et al., 2001a,b; Shelley, 2003; Lopez et al., 2002a,b). The remaining lipids are generated from $DC_{14}PC$ simply by adding or removing tail units (see Fig. 1) (Shelley et al., 2001b).

Fewer sites are used in the coarse-grain (CG) representation: in the case of DMPC, the CG model consists of 13 sites and 24 internal potentials—12 bonds and 12 bends; the all-atom CHARMM DMPC encompasses 118 atoms and 971 internal potentials—117 bonds, 226 bends, 315 torsions, and 313 one-fours. In addition, the soft interaction potentials allow a larger time step to be used and lead to enhanced diffusional and rotational motion (Lopez et al., 2002a,b; Whitehead et al., 2001). The simulation times given in this article are simply the number of time steps used multiplied by the time step size. However, lateral diffusion in the membrane plane occurs two orders of magnitude faster than this, so that a simulation time of 1 ns corresponds roughly to 100 ns of an all-atom simulation.

Peptide

The cylindrical assembly is aimed to mimic a small bundle of peptides or a macromolecular construct. The assembly is built as follows. Four rings of
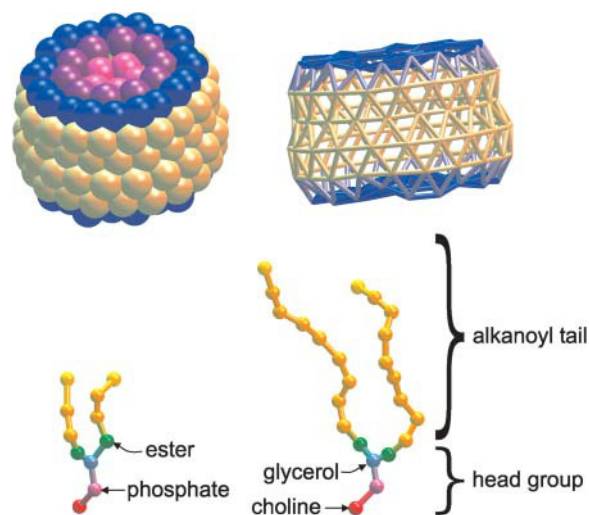

FIGURE 1   Snapshot of the model transmembrane peptide assembly showing the van der Waals radius (*top left*) and the skeletal bonding (*top right*) structures. The assembly is ~15 Å in radius and 20 Å long. The peptide consists of a hydrophobic cylinder capped with hydrophilic sites. The outer, middle, and inner capping rings are composed of identical sites, but have been colored differently (*blue/purple/pink*) for clarity. (*Bottom left*) The 11-site model of 1,2-di-undecanoyl-sn-glycero-3-phosphocholine ($DC_{11}PC$) and (*bottom right*) the 23-site model of $DC_{29}PC$. The choline and phosphate sites carry positive and negative electrostatic charges, respectively.

twenty hydrophobic sites are flanked by two rings of twenty hydrophilic sites to form the body of the cylinder. To cap the cylinder so that it is impenetrable and to increase the hydrophilicity of the cylinder ends, a 10-hydrophilic site middle ring and a 5-hydrophilic site inner ring are added to each end (see Fig. 1). In total there are 150 sites with 420 bond and 1950 bend potentials between them. Bonds are placed between all neighboring sites as shown in Fig. 1. There is a bend potential involving every triplet of atoms that are connected by bonds. All bonds and bends are harmonic with a force constant of 10,000 K. The equilibrium length and angle vary, however. All bonds have $r_{eq} = 4.65$ Å except for the inner hydrophilic ring intraring bonds, which have $r_{eq} = 6.50$ Å. All bends have $\theta_{eq} = 135°$ with the following exceptions: $\theta_{eq} = 90°$ is used between a hydrophobic, an outer-ring hydrophilic, and a middle-ring hydrophilic site to hold the cylindrical cap in place; in addition, the inner hydrophilic ring intraring bends are chosen to be one of $\theta_{eq} = 108°$, $\theta_{eq} = 72°$, or $\theta_{eq} = 36°$, depending on which is appropriate from the geometry. The assembly is ~15 Å in radius and 20 Å long. By way of comparison, the mechanosensitive channel MscL consists of five α-helices surrounding a pore that is 30 Å in diameter (Betanzos et al., 2002). The hydrophobic and hydrophilic sites have intermolecular potentials identical to the lipid alkanoyl tail sites and the water sites, respectively. All the peptide sites have a mass of 160 atomic units and are uncharged.

Small systems

Seven different systems, each consisting of 160 lipids and 1500 water sites (which represent three water molecules each), were employed. Each system is run in the NPT ensemble at 1 atm and 313.15 K. The lipid composition of the seven systems consists of four single-lipid and three mixed-lipid systems. The four single-lipid systems are $DC_{11}PC$ (short lipid, S1), $DC_{14}PC$ (S2), $DC_{17}PC$ (S3), and $DC_{29}PC$ (long lipid, S4). The three mixed-lipid systems are composed of $DC_{11}PC$ and $DC_{29}PC$ in differing proportions and have a short/long lipid ratio of 1:1 (S5), 1:3 (S6), and 3:1 (S7), respectively.

The initial condition is prepared as follows. A pair of lipids of the same type is generated such that their tails just meet. The x-y plane is then tiled uniformly with this pair using a 9×9 grid of side length 75 Å. One pair is deleted from the grid to obtain 80 lipids per leaflet. The 1:1 mixed system is constructed by placing the long and short lipids on alternating sites of the lattice. The 1:3 and 3:1 mixed systems are generated by populating three out of every four consecutive lattice sites with one lipid species, with the remaining sites being reserved for the other species. The mixed systems thus generated have a width mismatch—this mismatch heals quickly after which the headgroups all align in the same z range in each leaflet. These systems were each simulated for 1 ns; we remind the reader that this corresponds to roughly 100 ns for the equivalent all-atom simulation.

The width of the resultant bilayers is determined as follows. Each headgroup density peak in Fig. 2 A is fitted with a three-parameter Gaussian in a very localized region around the maximum. Then the centers of the pair of Gaussians for a single curve are subtracted to give the width.

Large systems

Separately, a hydrated, equilibrated bilayer patch of short and long lipids was prepared. Then the short lipid system was pulled apart and the long lipid system compressed by rigid translation of each of the two leaflets and their associated water sites. This was done so that the headgroups occupied similar z positions. These systems were used to tile a large patch (see Fig. 4). More water was added to fill the box. The final system consisted of 208 short lipids, 208 long lipids, and 10,400 water sites and was simulated for 4.6 ns (L1).

The final configuration of this run was taken as the starting configuration of the peptide insertion procedure. An x-y location was identified where the local density of lipids was such that there was a slight surplus of short lipids within the peptide radius, and a slight deficiency of short lipids just outside the peptide radius. Thirteen short lipids (six upper leaflet, seven lower leaflet) and nine long lipids (six upper leaflet, three lower leaflet) were removed to make room for the peptide. Tails of remaining (mainly long)
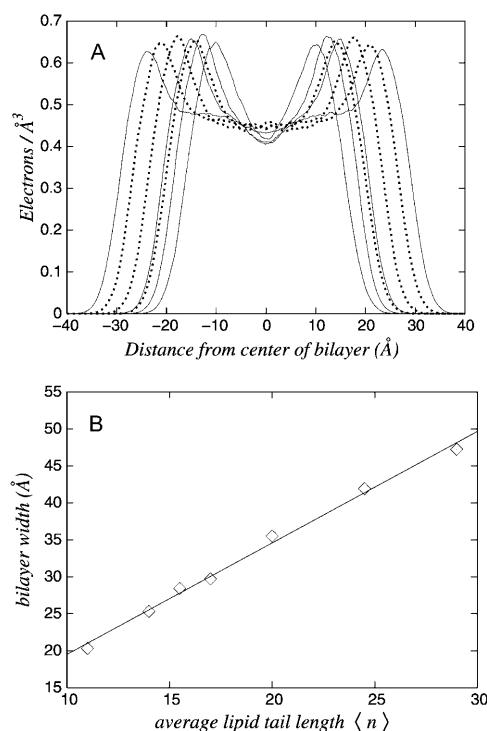

FIGURE 2 Panel A shows the lipid density distributions normal to the bilayer plane for the seven 160-lipid systems (S1–S7). Shown by solid line are the single-lipid systems and by dotted line the mixed-lipid systems. Panel B shows the bilayer width versus the average tail length (average n of the DC_nPC constituent lipids) of these systems. The best linear fit is also shown. The error bars are smaller than the symbols.

lipids that were still in the way were displaced slightly. Then the peptide was inserted. In addition, one upper leaflet short lipid and three lower leaflet long lipids were removed far from the peptide to balance the total number of lipids in each leaflet, and to balance the number of short and long lipids removed from each of the two leaflets, respectively. The peptide was frozen in place while the lipids and water were briefly allowed to relax around it. This system was then run for 10 ns (L2).

The starting configuration of the previous system (L2, with peptide) was taken and the water/lipid ratio was reduced to 25:1 (3450 waters, keeping in mind that one coarse grain site represents three water molecules) from 75:1 by removing water sites that were farthest from the lipids. The box length L_z was then reduced accordingly. This system was run for 10 ns (L3). Similarly, by reducing the x-y box size, two smaller peptide/water/lipid systems were generated and run for 10 ns. These consisted of 73 short lipids in each of the two leaflets, 74 long lipids in each of the two leaflets, and 2721 waters (L4); and 48 short lipids in each of the two leaflets, 50 long lipids in each of the two leaflets, and 1949 waters (L5).

Lastly, to demonstrate that the inverted phase transition also occurs in membranes composed of a single-lipid species, simulations were performed with the lipid $DC_{20}PC$. In this case, at a water/lipid ratio of 25:1, the threshold lipid/peptide ratio required for the phase transition is ~155:1.

RESULTS

Bilayer width determined by lipid composition

First we establish that the bilayer thickness, for our model, is predictable from the average length of the constituent lipids.

Seven separate bilayer systems were simulated (see Small systems, above). Four of these consisted of single-lipid systems, whereas three of them were taken to be mixtures of the longest and shortest lipid considered. The equilibrium lipid density for these systems is shown in Fig. 2 *A*. Notice that the single-lipid systems (S1–S4) all have a methyl trough region, whereas the mixed-lipid systems (S5–S7) have a flat or slightly inverted methyl trough region.

The mixed-lipid densities are broken down into the contributions from their constituent lipids in the three panels of Fig. 3. There are two features of note. The first is that the headgroups all occupy the same *z* plane – that is, the same plane parallel to the plane of the bilayer. The second is the hydrocarbon tail density. The determining factor for the bilayer width is the lipid-tail packing. The total tail density, irrespective of lipid identity, is similar in all cases, including the single-lipid systems (see Fig. 2 *A*). For the widest mixed-lipid bilayer (S6), the short lipids in either leaflet are completely separated from one another, as seen by the zero lipid density in Fig. 3 *A*. The long lipids bridge this depletion region with alkanoyl tail density, bringing the net density back up to its bulk value. For the intermediate mixed-lipid bilayer (S5), in which the two lipids are equally mixed (Fig. 3 *B*), the headgroup regions are seen to align perfectly, whereas the tail density for the short lipids is depleted in the middle of the bilayer. The long lipids once again fill the hydrocarbon region up to its bulk density value. For the shortest-width mixed-lipid bilayer (S7), the short lipid tails touch across leaflets, but their density is still depressed in the middle of the bilayer (see Fig. 3 *C*). The long lipid tails are severely

constrained in their extension normal to the bilayer plane and hence splay parallel to this plane, packing the middle of the bilayer up to its full tail density.

Finally, in Fig. 2 *B* the bilayer width is plotted against the average tail length of the constituent lipids. The relationship is linear, meaning that the width of the bilayer can be accurately selected by adjusting its lipid composition.

Lipid mixing in bilayer

For a two-component bilayer, consisting of otherwise identical lipids of differing tail length, the miscibility of the lipids depends upon the temperature. Domain formation in mixed bilayers is usually attributed to islands of the gel phase of the longer tail species in the gel-liquid region of the phase diagram (Gliss et al., 1998). We wish to study the effect of a membrane inclusion on an otherwise well-mixed system (Sens and Safran, 2000; Fattal and Ben-Shaul, 1993). Hence we first demonstrate that we are in the liquid-liquid region of the phase diagram where domain formation, in the absence of transmembrane peptides, is not observed (Dumas et al., 1997). It should be pointed out that all the lipids mentioned in the manuscript are in the fluid phase under the simulation conditions used. This is not in accordance with experiments and is due to the nature of the coarse-grained (CG) force field. See Nielsen et al. (2003) for a detailed discussion of alkane chain length.

A system consisting of 208 short lipids, 208 long lipids, and 10,400 water sites was prepared in a patchwork fashion (L1; see Fig. 4 and Large systems). This patchwork melts
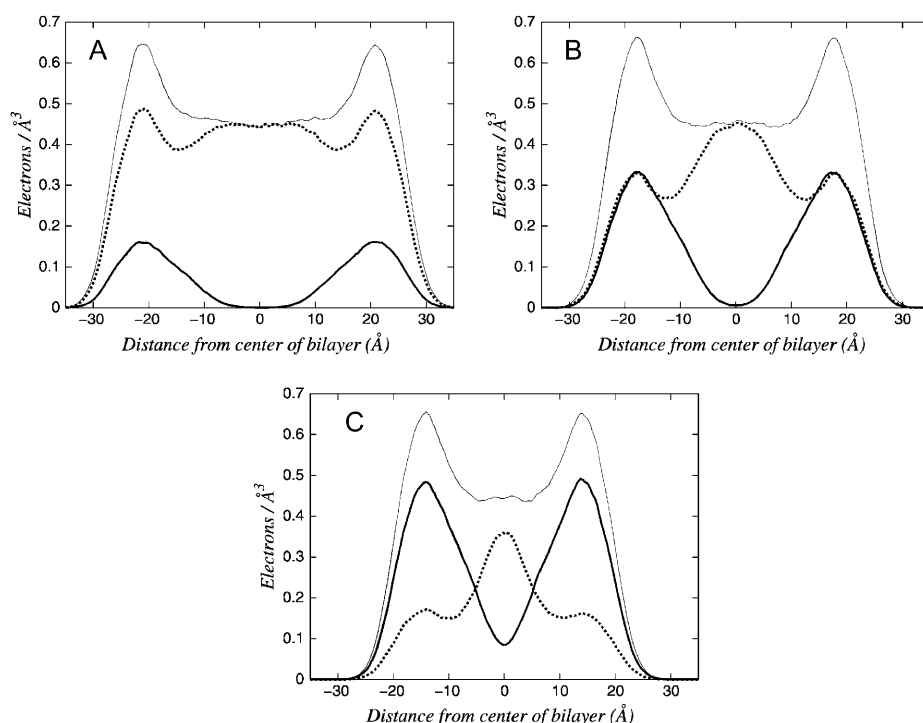
FIGURE 3 The lipid density distributions for the mixed-lipid systems (shown here in *solid line*) in Fig. 2 *A* are broken down into their constituent lipid densities. Panel *A* is for 40 short lipids and 120 long lipids (S6). Panel *B* is for 80 short lipids and 80 long lipids (S5). Panel *C* is for 120 short lipids and 40 long lipids (S7). The short lipids are shown in heavy solid line and the long lipids in dotted line.
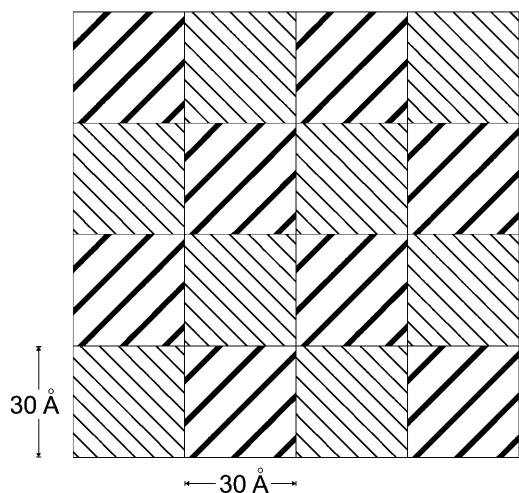
FIGURE 4 Schematic of the patchwork initial condition for the large mixed-lipid simulation (L1). Each patch, which includes both leaflets, contains only one of the two types of lipid.

and the two lipids mix. The extent of miscibility is quantified by calculating the three headgroup-headgroup center-of-mass two-dimensional radial distribution functions in the plane of the bilayer (see Fig. 5). From Peptides, above, we know that the headgroups align in the same z plane, so that we need only quantify miscibility in the x-y plane. It is seen in Fig. 5 that the lipids are completely miscible.

Peptide-induced mixed-lipid domain separation

The short peptide depicted in Fig. 1 is inserted into the mixed bilayer discussed in the preceding section (L2, as described in Large systems). With enough water so that the bilayer images are well separated, the role of the short peptide is to induce the formation of a meniscus (de Planque et al., 1998). The meniscus then drives the lipids to segregate on the basis of hydrophobic mismatch. The concentration of lipids around the peptide is initially slightly enriched in the long species as shown in Fig. 6 A. This is done deliberately so as not to bias the domain formation, since we eventually expect the short

lipid to collect around the peptide. A meniscus forms in the vicinity of the peptide as depicted in Fig. 7. The lipids residing next to the peptide, at a distance of roughly 15 Å from its center (see Fig. 7), are maximally perturbed from their equilibrium position. The mismatch is roughly 7.5 Å for each of the two bilayer leaflets. The lipids closer to the peptide are farther away from the bilayer center because they reside with their headgroups immediately above (for the upper leaflet) the hydrophilic peptide cap, with their alkanoyl tails bent to flank the length of the hydrophobic core of the peptide. After 10 ns of simulation, domain formation is clearly seen. The lipid species are distributed around the peptide as shown in Fig. 6 B. The region within 30 Å of the peptide center is enriched in the short-lipid species.

Peptide-induced multilamellar-to-inverted phase transition

For the typical 1,2-di-n-alkanoyl-sn-glycero-3-phosphocholine L_{α} water/lipid ratio of around 25:1, the role of the short peptide is more complicated. In the 400:1 lipid/peptide system (L3, see Large systems for the construction of the 400:1, 300:1, and 200:1 systems) a meniscus forms around each end of the peptide similar to that seen in Fig. 7. Water, which before the meniscus formed was distributed in a uniformly thick layer between the bilayers, accumulates in the meniscus region and is depleted from the regions far from the peptide (and its periodic images). In the 300:1 system (L4) this depletion is significant enough for the bilayers to come into contact midway between the peptides, pinching off most of the water into cylindrical pores. The system remains trapped in a defective state where water, lipid headgroups, and lipid tails mingle together as shown in Fig. 8. In the 200:1 system (L5) these defects heal as the lipid headgroups rearrange to solvate the water pores, and the remaining water migrates into the pore region. The process is shown in Fig. 9, A–C, and the final phase is shown from a different perspective in Fig. 9 D to show a perspective view of the cylindrical water pores. These results are consistent with experiment in the sense that the transition to an inverted
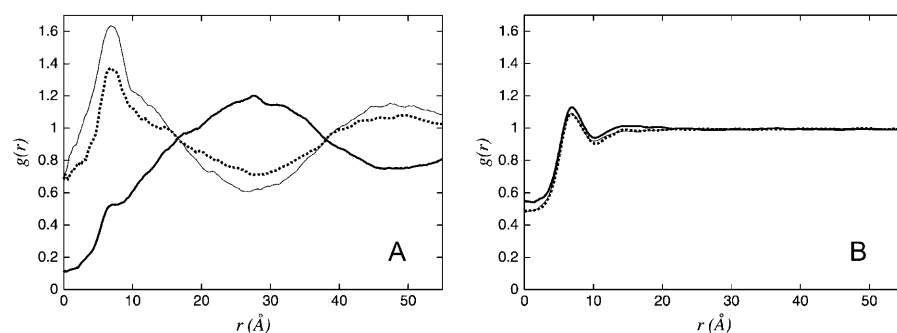

FIGURE 5 Two-dimensional lipid-lipid radial distribution functions (RDFs) in the bilayer plane for the simulation whose initial condition is shown in Fig. 4 (L1). Panel A shows the initial distribution taken from the first 50 ps of the simulation. Panel B shows the equilibrated distribution taken from the last 1 ns of the MD simulation. The short lipid-short lipid RDF is shown in solid line, the long lipid-long lipid RDF in dotted line, and the short lipid-long lipid RDF in heavy solid line. The lipid location is taken to be the center of mass of the headgroup. Both leaflets are included, which is the reason the distributions do not go to zero at zero (projected) separation.
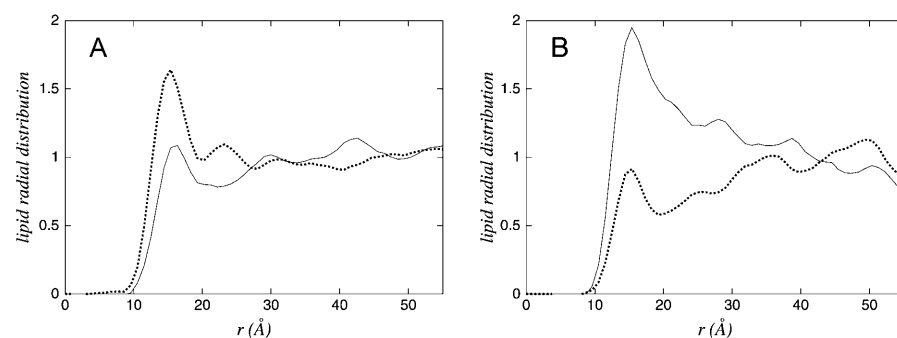
FIGURE 6 Two-dimensional radial distribution of lipids around the transbilayer peptide (system L2). Panel *A* shows the distribution immediately after the the peptide is inserted. The insertion location was chosen to correspond to a region of local enhancement of the long-lipid species. Panel *B* shows the distribution taken from the last 1 ns of the MD simulation. The short lipid is denoted by solid line, and the long lipid by dotted line. The lipid location is taken to be the center of mass of the headgroup. The peptide location is taken to be its center of mass. Both leaflets are included.

phase is only observed at high peptide/lipid ratios. The peptide concentration controls the phase transition through the extent of interbilayer water depletion caused by the meniscus regions. If we think of the water farthest from the peptide as a reservoir (e.g., the corner regions in the unit cell in Fig. 9 *A*) from which the meniscus region is filled, the depletion of the reservoir is negligible if the peptide concentration is extremely small. However, at higher and higher concentration, the reservoir region becomes smaller and smaller, until it does not contain enough water to fill the meniscus. The three concentrations we chose to study are representative of the different possible scenarios. We would like to stress that the L_α phase is stable in the absence of peptide.

The three scenarios described above also characterize systems containing only a single-lipid species. For the lipid $DC_{20}PC$, which forms bilayers of the same thickness as the mixed $DC_{11}PC$-$DC_{29}PC$ bilayers (L1–L5), the threshold lipid/peptide ratio needed to observe the formation of an inverted phase shifts down to ∼155. This shift is due in part to the domain segregation in the mixed-lipid case. The regions of the bilayer that are depleted of water gradually become enriched in the long lipid by the domain formation process. This facilitates the membrane fusion event since the long tail lipids tend to increase the bilayer width, which tends to push water out of the interbilayer region.

Before the bilayers come into contact, the water subphase extends in the *x* and *y* directions (the directions parallel to the membrane plane) in an infinite two-dimensional sheet. The initial contact is localized, with the bilayers only connected by a thin stalk. The water at this point is not segregated into the tubular domains shown in Fig. 9 *D* but rather forms a cross-hatched pattern in which the tubes are connected to one another. This is shown in the top panels of Fig. 10 immediately after membrane contact. Over time, however, a spontaneous symmetry breaking occurs, as shown in the bottom panels of Fig. 10, resulting in the final phase shown in Fig. 9 *D*.

The inverted unit cells are not isotropic in the sense that the position of a lipid in the cell affects how much room it has for its tail to stretch out (Harper et al., 2001). It has been argued that the short peptides occupy the shortest distance between water pores, relieving the longer alkanoyl lipid tails from having to pack into this geometry, and allowing them to occupy the more spacious ''corner'' regions where their tails can stretch out more (May and Ben-Shaul, 1999; Killian et al., 1996).

CONCLUSIONS

The hydrophobic matching principle has been shown to drive domain formation in a bilayer of otherwise miscible
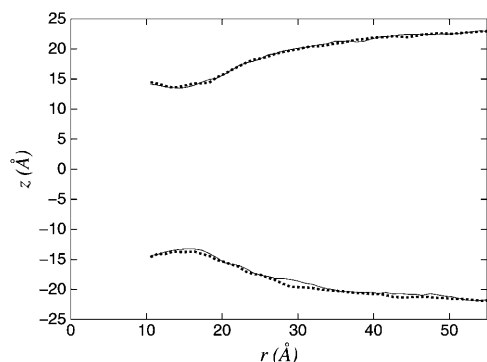

FIGURE 7 Extent of the lipid meniscus formed around the transbilayer peptide assembly (system L2). Separately for each of the two leaflets and each of the two lipid species, the average lipid headgroup center of mass height *z* (normal to the bilayer plane) relative to the peptide assembly center of mass is computed in the radial region in the membrane plane *r* to $r + \Delta r$, where $r = 0$ corresponds to the center of the peptide assembly. The short lipid is denoted by solid line and the long lipid by dotted line. The two leaflets appear as positive and negative height values.
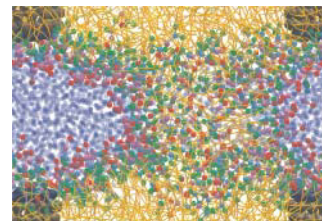

FIGURE 8 Snapshot of the defective inverted phase formed from the 300:1 lipid/peptide system (L4). Compare to Fig. 9, which shows the defect-free 200:1 system. Coloring is as follows: water, blue; lipids, as in Fig. 1; peptide darkened for clarity.
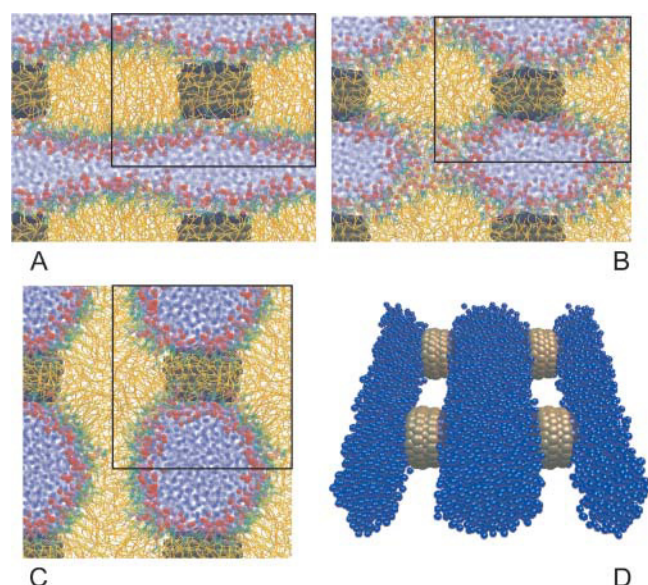
FIGURE 9 The L_α-to-inverted phase transition for the 200:1 lipid/peptide system (L5) is shown in panels *A–C*, with the simulation unit cell shown as a black rectangle. In panel *A* the meniscus induced by the peptide is evident. Accretion of interbilayer water into the meniscus allows for membrane contact (*B*). The lipid headgroups then rearrange to solvate the newly formed water pores (*C*). Coloring is as follows: water, blue; lipids as in Fig. 1; peptide darkened for clarity. Panel *D* shows a perspective view of the cylindrical water pores to further illustrate the structure of the inverted phase. All lipids have been removed for clarity.

FIGURE 10 Spontaneous symmetry breaking of the water network during the inverted phase transition (system L5). In the L_α phase the water is arranged in two-dimensional slabs in which the two directions are equivalent. The introduction of the peptide and the subsequent membrane contact does not break this symmetry, as seen immediately after fusion in the top panels. However, during the subsequent evolution this symmetry is spontaneously broken, as shown in the bottom panels.

lipids, and is responsible for the lamellar-to-inverted phase transition observed at high peptide concentration. This phase transition occurred in a mixed-lipid system; the transition was also demonstrated in a single-component lipid system by the same mechanism. However, the transition is slightly easier in the mixed-lipid case for two reasons. First, the regions of the bilayer that are depleted of water gradually become enriched in the long lipid by the domain formation process. This facilitates the membrane fusion event since the long tail lipids tend to increase the bilayer width, thus providing another force that tends to push water out of the interbilayer region. Second, since the inverted phase does not present an isotropic environment for the lipids, having different lipid species present helps to lessen the free-energy penalty of this anisotropy.

The domain formation induces a nonhomogeneous lipid concentration field around the peptide. In a lattice Monte Carlo simulation (Wahab et al., 2001) it was found that if two such regions with nonhomogeneous concentration fields overlap, an attractive force between the peptides results (Gil et al., 1998). The pair potential for this indirect force can be obtained from the free energy of the system, which depends on the distance between the peptides. We are currently investigating lipid-mediated peptide-peptide forces by placing more than one peptide assembly in the simulation cell. This would also allow for the possibility of forming an inverse hexagonal phase.
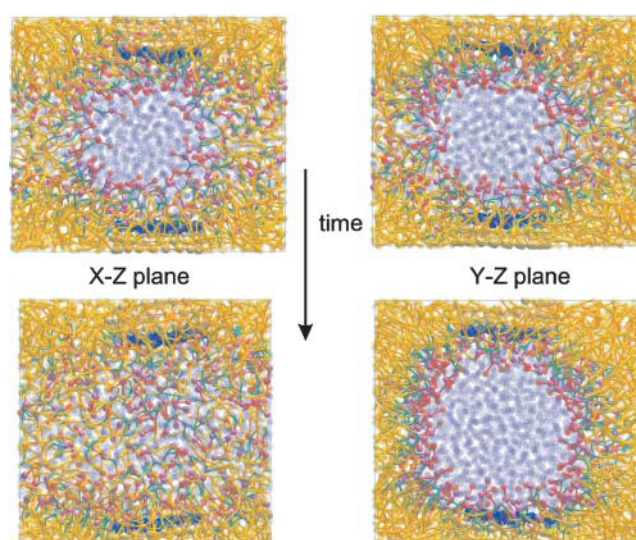
This study illustrates the use of the coarse-grain methodology as a testing ground for exploring the effect of individual physically motivated concepts in isolation from the full complexity of the problem. In conclusion, the mechanism we observe causes local water depletion to instigate membrane contact. Dehydration has the same effect—the likelihood of contact is increased. Heating increases the amplitude of the membrane undulations and bending fluctuations, again making contact likely (Goetz et al., 1999). In membrane protein crystallization the addition of salt, in the route reviewed by Caffrey, causes dehydration (Caffrey, 2000). The addition of cations can also be rationalized in terms of water depletion. The presence of lipids of negative intrinsic curvature lowers the barrier for the initial stalk formation because, for example in this case, the curvature due to the peptide-induced meniscus is positive and is hence highly unfavorable. We have demonstrated that with a deep meniscus and a high peptide/lipid ratio, we can induce an inverted phase transition even with phosphocholine lipids. We propose that the observed mechanism is largely responsible for the experimentally observed synthetic peptide-induced phosphocholine lipid lamellar-to-inverse hexagonal phase transition.

REFERENCES

Betanzos, M., C. S. Chiang, H. R. Guy, and S. Sukharev. 2002. A large iris-like expansion of a mechanosensitive channel protein induced by membrane tension. *Nat. Struct. Biol.* 9:704–710.

Caffrey, M. 2000. A lipid's eye view of membrane protein crystallization in mesophases. *Curr. Opin. Struct. Biol.* 10:486–497.

Dan, N., P. Pincus, and S. A. Safran. 1993. Membrane-induced interactions between inclusions. *Langmuir.* 9:2768–2771.

de Planque, M. R. R., E. Goormaghtigh, D. V. Greathouse, R. E. Koeppe II, J. A. W. Kruijtzer, R. M. J. Liskamp, B. de Kruijff, and J. A. Killian. 2001. Sensitivity of single membrane-spanning α-helical peptides to hydrophobic mismatch with a lipid bilayer: effects on backbone structure, orientation, and extent of membrane incorporation. *Biochemistry.* 40:5000–5010.

de Planque, M. R. R., D. V. Greathouse, R. E. Koeppe II, H. Schäfer, D. Marsh, and J. A. Killian. 1998. Influence of lipid/peptide hydrophobic mismatch on the thickness of diacylphosphatidylcholine bilayers. A ^{2}H NMR and ESR study using designed transmembrane α-helical peptides and gramicidin A. *Biochemistry.* 37:9333–9345.

Dumas, F., M. C. Lebrun, and J.-F. Tocanne. 1999. Is the protein/lipid hydrophobic matching principle relevant to membrane organization and functions? *FEBS Lett.* 458:271–277.

Dumas, F., M. M. Sperotto, M.-C. Lebrun, J.-F. Tocanne, and O. G. Mouritsen. 1997. Molecular sorting of lipids by bacteriorhodopsin in dilauroylphosphatidylcholine/distearoylphosphatidylcholine lipid bilayers. *Biophys. J.* 73:1940–1953.

Duque, D., X. Li, K. Katsov, and M. Schick. 2002. Molecular theory of hydrophobic mismatch between lipids and peptides. *J. Chem. Phys.* 116:10478–10484.

Fattal, D. R., and A. Ben-Shaul. 1993. A molecular model for lipid-protein interaction in membranes: the role of hydrophobic mismatch. *Biophys. J.* 65:1795–1809.

Finegold, L. 1993. Cholesterol in Membrane Models. CRC Press, Boca Raton.

Gil, T., J. H. Ipsen, O. G. Mouritsen, M. C. Sabra, M. M. Sperotto, and M. J. Zuckerman. 1998. Theoretical analysis of protein organization in lipid membranes. *Biochim. Biophys. Acta.* 1376:245–266.

Gliss, C., H. Clausen-Schaumann, R. Günther, S. Odenbach, O. Randl, and T. M. Bayerl. 1998. Direct detection of domains in phospholipid bilayers by grazing incidence diffraction of neutrons and atomic force microscopy. *Biophys. J.* 74:2443–2450.

Goetz, R., G. Gompper, and R. Lipowsky. 1999. Mobility and elasticity of self-assembled membranes. *Phys. Rev. Lett.* 82:221–224.

Gopal, A., and K. Y. C. Lee. 2001. Morphology and collapse transitions in binary phospholipid monolayers. *J. Phys. Chem. B.* 105:10348–10354.

Harper, P. E., D. A. Mannock, R. N. A. H. Lewis, R. N. McElhaney, and S. M. Gruner. 2001. X-ray diffraction structures of some phosphatidyl-ethanolamine lamellar and inverted hexagonal phases. *Biophys. J.* 81:2693–2706.

Harroun, T. A., W. T. Heller, T. M. Weiss, L. Yang, and H. W. Huang. 1999a. Experimental evidence for hydrophobic matching and membrane-mediated interactions in lipid bilayers containing gramicidin. *Biophys. J.* 76:937–945.

Harroun, T. A., W. T. Heller, T. M. Weiss, L. Yang, and H. W. Huang. 1999b. Theoretical analysis of hydrophobic matching and membrane-mediated interactions in lipid bilayers containing gramicidin. *Biophys. J.* 76:3176–3185.

Killian, J. A., I. Salemink, M. R. R. de Planque, G. Lindblom, R. E. Koeppe II, and D. V. Greathouse. 1996. Induction of nonbilayer structures in diacylphosphatidylcholine model membranes by transmembrane α-helical peptides: importance of hydrophobic mismatch and proposed role of tryptophans. *Biochemistry.* 35:1037–1045.

Kralchevsky, P. A., and K. Nagayama. 2000. Capillary interactions between particles bound to interfaces, liquid films and biomembranes. *Adv. Colloid. Interfac. Sci.* 85:145–192.

Lagüe, P., M. J. Zuckermann, and B. Roux. 1998. Protein inclusion in lipid membranes: a theory based on the hypernetted chain integral equation. *Faraday Discuss.* 111:165–172.

Lagüe, P., M. J. Zuckermann, and B. Roux. 2001. Lipid-mediated interactions between intrinsic membrane proteins: dependence on protein size and lipid composition. *Biophys. J.* 81:276–284.

Li, L. 2000. Relating helix tilt in a bilayer to lipid disorder: a mean-field theory. *Biophys. Chem.* 86:79–83.

Li, X., and M. Schick. 2000. Fluctuations in mixtures of lamellar- and nonlamellar-forming lipids. *J. Chem. Phys.* 112:10599–10607.

Lopez, C. F., P. B. Moore, J. C. Shelley, M. Y. Shelley, and M. L. Klein. 2002a. Computer simulation studies of biomembranes using a coarse grain model. *Comput. Phys. Commun.* 147:1–6.

Lopez, C. F., S. O. Nielsen, P. B. Moore, J. C. Shelley, and M. L. Klein. 2002b. Self-assembly of a phospholipid Langmuir monolayer using coarse-grained molecular dynamics simulations. *J. Phys. Condens. Matter.* 14:9431–9444.

Marrink, S., and A. E. Mark. 2003. The mechanism of vesicle fusion as revealed by molecular dynamics simulations. *J. Am. Chem. Soc.* 125:11144–11145.

May, S., and A. Ben-Shaul. 1999. Molecular theory of lipid-protein interaction and the L_α-H_{II} transition. *Biophys. J.* 76:751–767.

Nielsen, C., M. Goulian, and O. S. Andersen. 1998. Energetics of inclusion-induced bilayer deformations. *Biophys. J.* 74:1966–1983.

Nielsen, S. O., C. F. Lopez, G. Srinivas, and M. L. Klein. 2003. A coarse grain model for n-alkanes parameterized from surface tension data. *J. Chem. Phys.* 119:7043–7049.

Nielsen, S. O., C. F. Lopez, G. Srinivas, and M. L. Klein. 2004. Coarse grain models and the computer simulation of soft materials. *J. Phys. Condens. Matter.* 16:R481–R512.

Ortiz, A., J. A. Killian, A. J. Verkleij, and J. Wilschut. 1999. Membrane fusion and the lamellar-to-inverted-hexagonal phase transition in cardiolipin vesicle systems induced by divalent cations. *Biophys. J.* 77:2003–2014.

Petrache, H. I., D. M. Zuckerman, J. N. Sachs, J. A. Killian, R. E. Koeppe II, and T. B. Woolf. 2002. Hydrophobic matching mechanism investigated by molecular dynamics simulations. *Langmuir.* 18:1340–1351.

Rappolt, M., A. Hickel, F. Bringezu, and K. Lohner. 2003. Mechanism of the lamellar/inverse hexagonal phase transition examined by high resolution x-ray diffraction. *Biophys. J.* 84:3111–3122.

Safran, S. A. 1994. Statistical Thermodynamics of Surfaces, Interfaces, and Membranes. Addison-Wesley, New York.

Schief, W. R., L. Touryan, S. B. Hall, and V. Vogel. 2000. Nanoscale topographic instabilities of a phospholipid monolayer. *J. Phys. Chem. B.* 104:7388–7393.

Scott, H. L. 2002. Modeling the lipid component of membranes. *Curr. Opin. Struct. Biol.* 12:495–502.

Sens, P., and S. A. Safran. 2000. Inclusions induced phase separation in mixed lipid film. *Eur. Phys. J. E.* 1:237–248.

Sharpe, S., K. R. Barber, C. W. M. Grant, D. Goodyear, and M. R. Morrow. 2002. Organization of model helical peptides in lipid bilayers: insight into the behavior of single-span protein transmembrane domains. *Biophys. J.* 83:345–358.

Shelley, J. C. 2003. Modified coarse grain parameters for MD simulations in the NPT ensemble. www.cmm.upenn.edu.

Shelley, J. C., M. Y. Shelley, R. C. Reeder, S. Bandyopadhyay, and M. L. Klein. 2001a. A coarse grain model for phospholipid simulations. *J. Phys. Chem. B.* 105:4464–4470.

Shelley, J. C., M. Y. Shelley, R. C. Reeder, S. Bandyopadhyay, P. B. Moore, and M. L. Klein. 2001b. Simulations of phospholipids using a coarse grain model. *J. Phys. Chem. B.* 105:9785–9792.

Sprong, H., P. van der Sluijs, and G. van Meer. 2001. How proteins move lipids and lipids move proteins. *Nat. Rev. Mol. Cell Biol.* 2:504–513.

van der Wel, P. C. A., T. Pott, S. Morein, D. V. Greathouse, R. E. Koeppe II, and J. A. Killian. 2000. Tryptophan-anchored transmembrane peptides

promote formation of nonlamellar phases in phosphatidylethanolamine model membranes in a mismatch-dependent manner. *Biochemistry.* 39:3124–3133.

Wahab, M., H.-J. Mögel, and P. Schiller. 2001. Indirect interaction of inclusions in mixed membranes. *Mol. Phys.* 99:2045–2053.

Weikl, T. R. 2001. Fluctuation-induced aggregation of rigid membrane inclusions. *Europhys. Lett.* 54:547–553.

Whitehead, L., C. M. Edge, and J. W. Essex. 2001. Molecular dynamics simulation of the hydrocarbon region of a biomembrane using a reduced representation model. *J. Comput. Chem.* 22:1622–1633.

Yang, L., and H. W. Huang. 2002. Observation of a membrane fusion intermediate structure. *Science.* 297:1877–1879.

Zimmerberg, J., and L. V. Chernomordik. 1999. Membrane fusion. *Adv. Drug Deliv. Rev.* 38:197–205.